



# Coulomb distortion effects in quasi-elastic ( $e, e'$ ) scattering on heavy nuclei

Andreas Aste

*Department of Physics, University of Basel, Klingelbergstrasse 82, 4056 Basel, Switzerland*

Received 13 November 2007; received in revised form 18 March 2008; accepted 19 March 2008

Available online 22 March 2008

---

## Abstract

The influence of the Coulomb distortion for quasi-elastic ( $e, e'$ ) scattering on highly charged nuclei is investigated in distorted wave Born approximation for electrons. The Dirac equation is solved numerically in order to obtain exact electron continuum states in the electrostatic field generated by the charge distribution of an atomic nucleus. Different approximate models are used to describe the nucleon current in order to show that, at high electron energies and energy–momentum transfer, the influence of Coulomb distortions on ( $e, e'$ ) cross sections can be reliably described by the effective momentum approximation, irrespective of details concerning the description of the nuclear current.

© 2008 Elsevier B.V. All rights reserved.

PACS: 25.30.Fj; 25.70.Bc; 11.80.Fv

Keywords: Quasi-elastic electron scattering; Effective momentum approximation; Nucleon form factors; Coulomb corrections

---

## 1. Introduction

Quasi-elastic electron scattering on nuclei has represented during nearly three decades one of the most successful tools to study the nuclear and nucleon structure. Experiments have been performed at SLAC [1–3], the MIT Bates Laboratory [4–12], the Saclay Laboratory [13–18], and more recently at JLab in order to explore this reaction. Both inclusive ( $e, e'$ ) and exclusive (single arm ( $e, e'N$ ) or double arm ( $e, e'NN$ )) experiments contributed to a deeper understanding of the

---

*E-mail address:* [andreas.aste@unibas.ch](mailto:andreas.aste@unibas.ch).

many-body structure of strongly interacting systems like light and heavier nuclei opening the possibility of investigating also the *in-medium* nucleon properties.

Inclusive ( $e, e'$ ) scattering, where only the scattered electron is observed, provides information on a number of interesting nuclear properties like, e.g., the nuclear Fermi momentum [19], high-momentum components in nuclear wave functions [20], modifications of nucleon form factors in the nuclear medium [21,22], the scaling properties of the quasi-elastic response allow to study the reaction mechanism [23], and extrapolation of the quasi-elastic response to infinite nucleon number  $A = \infty$  provides us with a very valuable observable of infinite nuclear matter [24].

However, experimental studies of inclusive and exclusive reactions induced by electrons are hampered in the case of target nuclei with a large number of protons by the strong Coulomb field, which induces a distortion of the electron wave front, hereby modifying the structure of the ( $e, e'$ ) cross section and inducing sizable effects in the longitudinal and transverse separation of the electromagnetic response [25–29].

Still, there is a considerable theoretical and experimental interest in extracting longitudinal and transverse structure functions as a function of energy loss for fixed three momentum transfer for a range of nuclei. One of the important topics mentioned above concerning the in-medium modification of the nucleon form factors is related to the question whether the Coulomb sum rule is violated in nuclei. This sum rule states that the number of protons in a nucleus can be obtained from an integral of the electric response of the nucleus over the full range of the electron energy loss at large three-momentum transfer [22]. Unfortunately, the conclusions reached by the large experimental programs carried out at Bates, Saclay and SLAC for a variety of nuclei ranged from a full saturation of the Coulomb sum rule to its violation by 30%.

The approval of the Thomas Jefferson National Accelerator Facility (TJNAF) Proposal E01-016, entitled ‘Precision measurement of longitudinal and transverse response functions of quasi-elastic electron scattering in the momentum transfer range  $0.55 \text{ GeV} \leq |\vec{q}| \leq 1.0 \text{ GeV}$ ’, resulted in experiments performed very recently in Hall A at TJNAF, using target nuclei like  $^4\text{He}$ ,  $^{12}\text{C}$ ,  $^{56}\text{Fe}$ , and  $^{208}\text{Pb}$ . In the present study, we therefore focus on the particular case of  $^{208}\text{Pb}(e, e')$  scattering. Preliminary calculations for  $^{56}\text{Fe}(e, e')$  show that the conclusions drawn below in the present study apply to heavy nuclei like  $^{56}\text{Fe}$  in an analogous manner as well.

Since the plane wave Born approximation (PWBA) for electrons is no longer adequate for the calculation of scattering cross sections in the strong and long-range electrostatic field of highly charged nuclei, it has become clear in recent years that the correct treatment of the Coulomb distortion of the electron wave function due to the electrostatic field of the nucleus is unavoidable if one aims at a consistent interpretation of experimental data. The theoretical framework to investigate Coulomb corrections to the electron–nucleus cross sections is well established and is called distorted wave Born approximation (DWBA) in contrast to the better known PWBA where the incoming and outgoing charged leptons are described by (Dirac) plane waves, neglecting the effect of the Coulomb interaction between the projectile and the target nucleus. The application of the DWBA scheme is in principle straightforward, but the numerical complications lead to extremely time consuming calculations.

DWBA calculations with exact Dirac wave functions have been performed by Kim et al. [30] in the Ohio group and Udias et al. [31,32] for inclusive quasi-elastic scattering on heavy nuclei. However, these cumbersome calculations are difficult to control by people who were not directly involved in the development of the respective programs. Early DWBA calculations for  $^{12}\text{C}$  and  $^{40}\text{Ca}$  were presented in [26]. Coulomb corrections have also been evaluated theoretically by a group from Trento University [33], where it was found that the standard method (used mainly in the case of light nuclei) to handle Coulomb distortions for elastic scattering in data analysis,

the so-called effective momentum approximation (EMA), works with an accuracy better than 1% for the description of Coulomb distortion effects, if the energy of the scattered electrons and the momentum transfer is sufficiently high. On the other hand, the Ohio group derived significant corrections beyond the EMA. The findings presented in this paper confirm that the conclusions drawn by the Trento group are basically correct. There is a certain mismatch between the EMA and exact calculations for small energy transfer, which, however, strongly decreases when the energy transfer becomes significantly larger than the typical removal energy of the bound nucleons.

Calculations using an eikonal approximation (called eikonal distorted wave Born approximation, EDWBA) for electrons have been performed by the Basel group [34,35], which seemed to confirm the results of the Ohio group. However, a poor approximation for the focusing of the electrons near the nucleus was used, leading to an overestimation of the Coulomb corrected cross sections. Through a subsequent analysis using exact electron wave functions we found that the eikonal approximation with an improved non-perturbative description of the electron wave function amplitude supports the observation that the EMA is indeed a valid tool for the description of Coulomb distortion effects [36]. A similar preliminary result was obtained in [37], where exact solutions of the Dirac equation were used for the electron wave functions. The nuclear current was modeled within the framework of a simplified single particle shell (SPS) model, with harmonic oscillator wave functions for the bound nucleons and plane waves for the knocked-out nucleons. The cross section for inclusive quasi-elastic scattering process is usually calculated approximately by summing over all knock-out processes, where the individual bound nucleons inside the nucleus leave the nucleus after a sufficiently high energy transfer  $\omega = \epsilon_i - \epsilon_f$  from the scattered electron, where  $\epsilon_i$  is the initial and  $\epsilon_f$  the final electron energy. The recoil nucleons move in an energy dependent optical potential. It is common practice that the imaginary part of the optical potential is not taken into account in the calculations, since the imaginary part is intended to describe the loss of nucleon flux inside the nuclear medium. In inclusive processes, only the electrons are observed, and one may argue that it is not necessary to take into account whether or not the recoil nucleons actually leave the nucleus or initiate some subsequent nuclear reactions. Still, it has been shown in [38] that  $(e, e')$  peak intensities are reduced by typically 5–10% as a result of final state interaction (FSI) for the kinematics relevant for this paper, and how this reduction is related to the imaginary part of the final state nucleon optical potential (see Eq. (29a) in [38]). The effects of the FSI at high momentum transfer have been discussed in [39].

In this paper, we present calculations based on two different models for the nuclear current. The electrons are described by exact solutions of the Dirac equation in our DWBA calculations. The final state nucleons are not described by wave functions obtained as solutions of the Dirac equation with some nuclear model potential. Instead, an eikonal approximation and the plane wave approximation are used, reducing the computational costs in a very effective way. It turns out that the use of approximate wave functions is not necessarily a weakness, since we find that at sufficiently high energies and momentum transfer, the effective momentum approximation provides an accurate description of Coulomb corrections, irrespective of the nuclear model used for the final state nucleons. It is a fact that also elaborate nuclear current models, based, e.g., on solutions of the Dirac equation for the nucleons in some relativistic nuclear model, cannot be considered as a fully satisfying strategy, as the still sizeable discrepancy between measured and calculated cross sections shows (see, e.g., [30]). Computational costs always restrain us from using more realistic nuclear models, where effects like nucleon correlations and meson exchange currents can be properly taken into account.

## 2. From DWBA to EMA

Inclusive ( $e, e'$ ) cross sections are usually calculated by integrating over all final state nucleons in the knock-out ( $e, e'N$ ) cross sections obtained from a single-particle shell model [40] for the bound protons and neutrons, as will be explained in further detail in the following section. The differential cross section for single nucleon knockout is given by [31]

$$\frac{d^4\sigma}{d\epsilon_f d\Omega_f dE_f d\Omega_F} = \frac{4\alpha^2}{(2\pi)^3} \epsilon_f^2 E_f p_f \delta(\epsilon_i + E_A - \epsilon_f - E_f - E_{A-1}) \overline{\sum} |W_{if}|^2, \quad (1)$$

with the matrix element

$$W_{if} = \frac{1}{(2\pi)^3} \int d^3r_e \int d^3r_N \int d^3q' \left[ j_\mu^e(\vec{r}_e) \frac{e^{-i\vec{q}'(\vec{r}_e - \vec{r}_N)}}{q'^2_\mu + i0} j_N^\mu(\vec{r}_N) \right], \quad (2)$$

where  $j_N^\mu(\vec{r}_N)$  is the nucleon transition current obtained within the framework of some suitable nuclear model, the  $\overline{\sum}$  in Eq. (1) indicates the sum (average) over final (initial) polarizations, and  $E_A, E_{A-1}$  is the energy of the initial and final nucleus, respectively. The virtuality of the exchanged photon is  $q'^2_\mu = \omega^2 - \vec{q}'^2$ , where  $q^0 = \omega = \epsilon_i - \epsilon_f$  is the energy transferred by the electron to the nuclear system. In our calculations, the final nucleus was considered as a spectator, and the final energy  $E_f$  of the nucleon was calculated from the energy transfer reduced by a reasonable separation (or removal) energy.

In the PWBA, the electron current is given by

$$j_e^\mu(\vec{r}_e) = \bar{u}_{s_f}(\vec{k}_f) \gamma^\mu u_{s_i}(\vec{k}_i) e^{i\vec{k}_i \vec{r}_e - i\vec{k}_f \vec{r}_e}, \quad (3)$$

where  $u_{s_i}, u_{s_f}$  are initial/final state plane wave electron spinors corresponding to the initial/final electron momentum  $\vec{k}_{i,f}$  and spin  $s_{i,f}$ , normalized according to

$$\bar{u}_s(\vec{k}) \gamma^0 u_{s'}(\vec{k}) = \delta_{s,s'}, \quad (4)$$

and a short calculation yields a three-dimensional integral

$$W_{if}^{\text{PWBA}} = -\frac{1}{Q^2} \int d^3r [j_\mu^e(\vec{r}) j_N^\mu(\vec{r})] \quad (5)$$

with the four-momentum transfer squared  $Q^2 = (\vec{k}_i - \vec{k}_f)^2 - \omega^2 = \vec{q}^2 - \omega^2$ .

In the DWBA, exact solutions of the Dirac equation for electrons in the electrostatic field of the nucleus are used instead of plane wave functions. In a general sense, the EMA accounts for the two effects of the Coulomb distortion, namely the momentum enhancement of the electron near the attractive nucleus and the focusing of the electron wave function. Therefore, transition amplitudes are calculated by replacing the asymptotic initial and final state momenta  $\vec{k}_i, \vec{k}_f$  of the electron by appropriate effective momenta in the PWBA transition amplitude. Additionally, the cross section obtained from the effective transition amplitude is multiplied by an appropriate focusing factor, which accounts for the fact that the electron wave function amplitude is enhanced in the vicinity of the nucleus, i.e. from a semiclassical point of view, the nucleus acts like a lens and concentrates the electrons towards the nuclear interior.

Indeed, one may establish a direct connection between the DWBA and the EMA. The DWBA transition amplitude comprises the exact solution of the Dirac equation for the electron in the electrostatic field of the nucleus. In this way, the DWBA accounts for the exchange of the ‘soft’

photons between electron and nucleus, whereas the explicit photon propagator in Eq. (2) accounts for the exchange of one hard photon.

Using the distributional identity

$$\int \frac{d^3q'}{(2\pi)^3} \frac{e^{i\vec{q}'\vec{r}}}{\omega^2 - \vec{q}'^2 \pm i0} = -\frac{e^{\pm i\omega r}}{4\pi r}, \quad (6)$$

one obtains

$$\begin{aligned} W_{if} &= -\frac{1}{4\pi} \int d^3r_e d^3r_N j_e^\mu(\vec{r}_e) j_\mu^N(\vec{r}_N) \frac{e^{i\omega|\vec{r}_e - \vec{r}_N|}}{|\vec{r}_e - \vec{r}_N|} \\ &= -\frac{1}{4\pi} \int d^3r_e d^3r_N \{ \rho_e(\vec{r}_e) \rho_N(\vec{r}_N) - \vec{j}_e(\vec{r}_e) \vec{j}_N(\vec{r}_N) \} \frac{e^{i\omega r}}{r}, \\ r &= |\vec{r}_e - \vec{r}_N|, \end{aligned} \quad (7)$$

with  $\rho_e, \rho_N, \vec{j}_e, \vec{j}_N$  denoting the transition charge and current densities of the electron and the nucleon, respectively. The double volume integral presents a clear numerical disadvantage of this expression. According to Knoll [41], one may introduce the scalar operator

$$S = e^{i\vec{q}\vec{r}} \sum_{n=0} \left( \frac{2i\vec{q}\vec{\nabla} + \Delta}{\vec{q}^2 - \omega^2} \right)^n e^{-i\vec{q}\vec{r}}, \quad \vec{q} = \vec{k}_i - \vec{k}_f, \quad (8)$$

such that the transition amplitude can be expanded in a more convenient form

$$W_{if} = -\frac{1}{Q^2} \int d^3r [\rho_N(\vec{r}) S \rho_e(\vec{r}) - \vec{j}_N S \vec{j}_e(\vec{r})]. \quad (9)$$

The single integral is limited to the region of the nucleus, where the nuclear current is relevant. The expansion Eq. (8) is an asymptotic one, in the sense that there is an optimum number (depending on  $\vec{q}$ ) of terms that give the best approximation to the exact value. Considering terms up to second order in the derivatives only one obtains

$$\begin{aligned} W_{if} &= -\frac{1}{Q^2} \int d^3r \left\{ \rho_N(\vec{r}) e^{i\vec{q}\vec{r}} \left[ 1 + \frac{2i\vec{q}\vec{\nabla} + \Delta}{Q^2} - \frac{4(\vec{q}\vec{\nabla})^2}{(Q^2)^2} \right] e^{-i\vec{q}\vec{r}} \rho_e(\vec{r}) \right. \\ &\quad \left. + \text{current terms} \right\}. \end{aligned} \quad (10)$$

This approximation has been used in our calculations [37] and in an equivalent way in [30], where it was also observed that higher order terms can indeed be neglected for the calculations relevant for this work. It should also be mentioned that the approximation has been applied for the first time to inclusive reactions in [27,28], and discussed in the context of the  $(e, e'p)$  quasi-elastic reaction in [42].

There is indeed a simple semiclassical interpretation of this expansion. If one assumes that the electron is scattered locally with a momentum transfer  $\vec{q}_{\text{loc}}(\vec{r}) = \vec{q} + \Delta\vec{q}(\vec{r})$ , calculable from the classical local momentum of the electron in the electrostatic potential and which deviates by  $\Delta\vec{q}$  from the asymptotic momentum transfer  $\vec{q}$ , then one has

$$\begin{aligned} \frac{Q^2}{Q_{\text{loc}}^2} &= \frac{\vec{q}^2 - \omega^2}{(\vec{q} + \Delta\vec{q})^2 - \omega^2} = \frac{Q^2}{Q^2 + 2\vec{q}\Delta\vec{q} + \Delta\vec{q}^2} \\ &= 1 - \frac{2\vec{q}\Delta\vec{q} + \Delta\vec{q}^2}{Q^2} + \frac{4(\vec{q}\Delta\vec{q})^2}{(Q^2)^2} + \dots \end{aligned} \quad (11)$$

Furthermore, one may note that the PWBA electron transition current can be written as

$$j_e^\mu(\vec{r}) = |j_e^\mu(\vec{r})| e^{i\vec{q}\vec{r}}. \tag{12}$$

Applying the operator  $\hat{q} = \frac{\vec{\nabla}}{i}$  on  $j_e^\mu(\vec{r})$  leads to  $\hat{q} j_e^\mu(\vec{r}) = \vec{q} j_e^\mu(\vec{r})$ , i.e.  $\frac{\vec{\nabla}}{i}$  acts as momentum transfer operator and replacing  $\vec{q}$  in (11) by  $\hat{q}$ , one immediately obtains the differential operator part of  $S$ .

Therefore, the Knoll operator  $S$  first factors out the undistorted  $e^{i\vec{q}\vec{r}}$ -term in the current, then calculates the ratio of the asymptotic momentum transfer with a quantity that can be interpreted as the local momentum transfer generated from the distorted electron current, and finally reinserts the  $e^{-i\vec{q}\vec{r}}$ -behavior of the undistorted current.

Assuming that one can approximate the effect of the  $S$ -operator by replacing it by an average (effective) momentum transfer  $Q_{\text{eff}}^2$ , one obtains as a first approximation for the transition matrix element

$$W_{if} = -\frac{1}{Q_{\text{eff}}^2} \int d^3r j_e^\mu(\vec{r}) j_\mu^N(\vec{r}), \tag{13}$$

keeping in mind that the DWBA electron current still has to be used in Eq. (13). Since a highly relativistic particle (with negligible mass  $m$ ) is moving nearly on a straight line, the classical momentum of a particle with asymptotic momentum  $\vec{k}$  and energy  $\sqrt{k^2 + m^2} \simeq |\vec{k}|$  moving inside a potential  $V(\vec{r})$  is given by  $\frac{\vec{k}}{|\vec{k}|}(k - V(\vec{r}))$ . Additionally, since the knockout process is nearly local for large momentum transfer (e.g.,  $Q^2 = (400 \text{ MeV})^2$  corresponds to a photon propagation length scale of  $\simeq \frac{1}{2}$  fm which is much smaller than the extension of a heavy nucleus), and since it takes place in the entire volume of the nucleus, it is self-evident that one should calculate  $Q_{\text{eff}}^2$  from a potential value  $\bar{V}$  which is obtained by an averaging process over the nuclear density profile  $\rho(\vec{r})$

$$Q_{\text{eff}}^2 = (\vec{k}_i^{\text{eff}} - \vec{k}_f^{\text{eff}})^2 - \omega^2, \quad \vec{k}_{i,f}^{\text{eff}} = \frac{\vec{k}_{i,f}}{|\vec{k}_{i,f}|}(k_{i,f} - \bar{V}) \tag{14}$$

with

$$\bar{V} \simeq \frac{\int d^3r \rho(\vec{r}) V(\vec{r})}{\int d^3r \rho(\vec{r})}, \tag{15}$$

where  $\rho$  can also be used for an approximate description of the charge density of the nucleus. In the case of a homogeneously charged sphere with radius  $R$  and charge number  $Z$ , the electric potential in the center of the sphere is given by  $V(0) = -\frac{3\alpha}{2R}$  ( $\alpha$  is the fine structure constant), whereas the potential averaged over the volume of the sphere is given by  $\bar{V} = 4V(0)/5$ .

A further approximation which can be made in Eq. (13) stems from the observation that the attractive nucleus focuses the electron wave function in the nuclear region. It can be shown that for highly relativistic energies, the amplitude of the initial/final state electron wave function in the nuclear center is enhanced by a focusing factor  $f_{i,f}(0) = (1 - V(0)/|\vec{k}_{i,f}|)$ , however, solving the Dirac equation for an electron in the electrostatic field of a highly charged nucleus again shows that the focusing averaged over the nuclear volume is again well described by  $f_{i,f} = (1 - \bar{V}/|\vec{k}_{i,f}|)$ . Since the electron transition current is given by  $j_e^\mu = \bar{\psi}_{e,f} \gamma^\mu \psi_{e,i}$ , one may replace  $j_e^\mu(\vec{r})$  by  $f_i^{\text{eff}} f_f^{\text{eff}} j_e^{\mu,\text{EMA}}$ , where  $j_e^{\mu,\text{EMA}}$  is calculated with plane electron waves with effective momenta. A detailed discussion of the focusing effect can be found in [43].

If the same average potential value  $\bar{V}$  is used to calculate the effective momenta and the effective focusing factors, then a short calculation shows that the focusing factors cancel against the effective photon propagator  $\sim Q_{\text{eff}}^{-4}$  in the cross section in the sense that

$$\frac{(f_i^{\text{eff}})^2 (f_f^{\text{eff}})^2}{Q_{\text{eff}}^4} = \frac{1}{Q^4}, \quad (16)$$

and consequently, the EMA cross section is calculated by replacing the electron current in (10) by the PWBA current calculated from the effective momenta, and leaving everything else unchanged. A different, but completely equivalent strategy is to calculate first the theoretical cross section based on the effective momenta and energies instead of the corresponding asymptotic values. The intermediate result obtained this way must be multiplied subsequently by  $(f_i^{\text{eff}})^2$  in order to account for the focusing of the incident electron. The focusing of the final state electron is automatically taken into account by the artificially enhanced phase space factor  $(\epsilon_f^{\text{eff}})^2 \sim |\vec{k}_f^{\text{eff}}|^2$ .

The cancellation mechanism that plays between the focusing effect and the photon propagator in the matrix element is accidental and not really exact. It works in a very satisfactory way for nuclear charge distributions which are close to the homogeneous, spherical case. If the energy of the final state electron becomes significantly smaller than 150 MeV and the four-momentum transfer is below  $(300 \text{ MeV})^2$ , the semiclassical picture on which the EMA is based starts to fail. Furthermore, for small energy transfer  $\omega$  comparable to the removal energy of the nucleons, details of the nuclear structure and the interaction of the recoil nucleons with the nuclear matter become increasingly important, which makes the applicability of the EMA questionable. However, this kinematical region is of minor interest in future experiments.

### 3. Models and approximations

#### 3.1. Single particle shell model

As mentioned before, inclusive  $(e, e')$  cross sections are commonly calculated by integrating over all final state nucleons in  $(e, e'N)$  cross sections obtained from a single-particle shell (SPS) model for the bound protons and neutrons. Usually, the fact that there are short-range and tensor correlations between nucleon pairs which lead to a partial depletion of the single particle shells is ignored in SPS  $(e, e')$  calculations. Within a correlated basis functions theory calculation, it was found in [44] for nuclear matter that there is an approximate probability of 20% for a nucleon being in an correlated state [45]. However, correlated nucleons account for approximately 37% of the average removal energy. In view of the fact that the average binding energy of, e.g., protons is 21 MeV in our SPS calculations, this observation implies that the correlated nucleons correspond to strongly bound particles with binding energies around 100 MeV, if an average removal energy of 37 MeV is assumed. The impact of correlated nucleons on the inclusive cross section is therefore strongly suppressed for an energy transfer clearly smaller than 150 MeV compared to the strength of the uncorrelated nucleons. Still, a reduction of  $\sim 20\%$  of the peak strength results from the suppression of correlated nucleons, combined with a slight shift of the peak towards higher energy transfer  $\omega$  and an increase of strength in the high- $\omega$  tail.

A further observation, which is of minor importance concerning the present calculations, is the fact that the rms radius of uncorrelated nucleons tends to be slightly larger than the total rms radius of the nucleus [45]. We therefore performed calculations within a strongly simplified framework, where the correlated (high-momentum) nucleons were described by model wave

functions with a high-momentum component and large binding energies. We found that even in this case, the EMA remains valid to an acceptable extent, if the ‘correlated’ nucleons are distributed in a reasonable homogeneous manner inside the nucleus, and if the momentum transfer and final electron energy are sufficiently large. In this work, we therefore focus on the main contribution of the uncorrelated nucleons in the region of the quasi-elastic peak, in order to facilitate a comparison to other works [30].

The relativistic form of the wave functions for bound protons and neutrons was constructed from the non-relativistic wave function. Non-relativistic bound nucleon wave functions were generated using a self-consistent Schrödinger solver for a non-relativistic Woods–Saxon potential and the additional Coulomb potential for the protons. The Woods–Saxon potential, which included an LS coupling term, was optimized in such a way that the experimental binding energies of the upper proton shells and the rms of the nuclear charge distribution were reproduced correctly. The standard way to construct nucleon four-spinors  $\psi_N$  from a Schrödinger-type nucleon wave function  $\chi_N$  was then applied, given by

$$\psi_N(\vec{x}) = N \left( \chi_N(\vec{x}), \frac{\vec{\sigma} \cdot \hat{p}}{\bar{E} + m_N} \chi_N(\vec{x}) \right), \quad (17)$$

where  $\hat{p}$  denotes the differential momentum operator,  $\bar{E}$  is the energy of the nucleon, and  $N$  is a normalization factor which is typically close to one. The same strategy, which is exact in the case of Dirac plane waves, was also applied to construct the small component of the Dirac spinor in the case of the nucleon eikonal approximation. For a discussion of this approximation we refer to [46].

The nuclear charge distribution, which is the main input for the calculation of the Dirac electron wave functions, and nucleon optical potentials of heavy nuclei are often approximated by the help of a Woods–Saxon distribution. Since the normalization and moments of Woods–Saxon distributions are rarely found in the literature, some important expressions are listed in Appendix A.

### 3.2. Eikonal approximation for nucleons

In order to generate realistic nucleon wave functions in a computationally efficient way, we used eikonal wave functions for the final state protons and neutrons, with the aim to compare the (Coulomb corrected) cross sections obtained from the eikonal nuclear model to the cross section obtained from simple nucleon plane wave calculations.

The eikonal phases  $\chi_{1,2}$  generated by a potential  $U(\vec{r})$  take the local (semiclassical) momentum modification of the incoming/outgoing nucleon with initial/final asymptotic momentum  $\vec{p}_{i,f} = |\vec{p}_{i,f}| \hat{p}_{i,f}$  approximately into account by modifying the plane waves describing the nucleons according to

$$e^{i\vec{p}_{i,f}\vec{r}} \rightarrow e^{i\vec{p}_{i,f}\vec{r} \pm i\chi_{1,2}(\vec{r})}, \quad (18)$$

where

$$\chi_1(\vec{r}) = -\frac{E_i}{|\vec{p}_i|} \int_{-\infty}^0 U(\vec{r} + \hat{p}_i s) ds, \quad z = \hat{p}_i \vec{r}, \quad (19)$$

or

$$\chi_1(\vec{r}) = -\frac{E_i}{|\vec{p}_i|} \int_{-\infty}^z U(x, y, z') dz', \quad z = \hat{p}_i \vec{r} \quad (20)$$



if the initial nucleon momentum is parallel to the  $z$ -axis. The eikonal phase for the final state relevant for the calculations presented in this work is

$$\chi_2(\vec{r}) = -\frac{E_f}{|\vec{p}_f|} \int_0^\infty U(\vec{r} + \hat{p}_f s') ds', \quad (21)$$

where  $E_{i,f} = (\vec{p}_{i,f}^2 + m_N^2)^{1/2}$  is the energy of the nucleon with mass  $m_N$ , and  $E_f/|\vec{p}_f|$  is the velocity of the knocked-out nucleon. An energy-dependent volume-central part of an optical Woods–Saxon type model potential  $V_{\text{nuc}}(r, E)$  as given in a recent work [47] was used for our calculations, as well as the energy-independent Woods–Saxon potential which was used to generate the bound state nucleon wave functions.

The total potential  $U(r, E) = V_{\text{nuc}}(r, E) + V_{\text{coul}}(r)$  is given as the sum of a Woods–Saxon potential and the Coulomb potential of the final state nucleus in the case of protons. The depth of the Woods–Saxon type nuclear potential

$$V_{\text{nuc}}(r, E) = -\frac{V_{\text{WS}}(E)}{1 + e^{(r-r_{\text{nuc}})/a_{\text{nuc}}}} \quad (22)$$

depending on the energy  $E$  of the proton (all quantities in MeV) is given by

$$V_{\text{WS}}(E) = v_1 [1 - v_2(E - E_f) + v_3(E - E_f)^2 - v_4(E - E_f)^3], \quad (23)$$

where  $E_f = -5.9$  and

$$v_1 = 67.2, \quad v_2 = 7.9 \times 10^{-3}, \quad v_3 = 2.0 \times 10^{-5}, \quad v_4 = 7 \times 10^{-9}, \quad (24)$$

whereas the parameters for neutrons are  $E_f = -5.65$  and

$$v_1 = 50.6, \quad v_2 = 6.9 \times 10^{-3}, \quad v_3 = 1.5 \times 10^{-5}, \quad v_4 = 7 \times 10^{-9}. \quad (25)$$

The range and diffusivity are both for protons and neutrons given by  $r_{\text{nuc}} = 7.371$  fm and  $a_{\text{nuc}} = 0.646$  fm according to [47].

The imaginary part of the optical potential, which is intended to describe the loss of flux in proton (neutron) elastic scattering, has been neglected in our ( $e, e'$ ) calculations. As mentioned in the introduction, in inclusive processes, only the electrons are observed, and the eventuality whether or not an ejected nucleons got ‘lost’, i.e. initiated some subsequent nuclear reaction, does not play a very important role. Furthermore, the FSI affects the inclusive cross sections in a similar way whether the electron wave function distortion is taken into account or not, such that a comparison of electron PWBA and DWBA calculations is still possible.

To calculate the eikonal integral for a Woods–Saxon potential numerically would be relatively time consuming, and unfortunately, the eikonal integral of a Woods–Saxon potential is not suitable for simple analytic estimations [48,49]. Therefore, one may approximate the Woods–Saxon shape of the mean-field optical nucleon potential  $V_{\text{nuc}}$  in an effective way by a power series in the distance from the nuclear center. We found that the following simple two-parameter approximation provides an efficient approximation for  $V_{\text{nuc}}(r)$  in the range  $0 < r < R_{\text{max}}$  in the case of  $^{208}\text{Pb}$ , where  $R_{\text{max}} = 10$  fm:

$$\tilde{V}_{\text{nuc}}(r, E) = -V_{\text{WS}}(E) + c_1(E)r^7 + c_2(E)r^6 \quad (26)$$

with

$$c_1 = -6 \frac{V_{\text{WS}}}{R_{\text{max}}^7}, \quad c_2 = 7 \frac{V_{\text{WS}}}{R_{\text{max}}^6}. \quad (27)$$

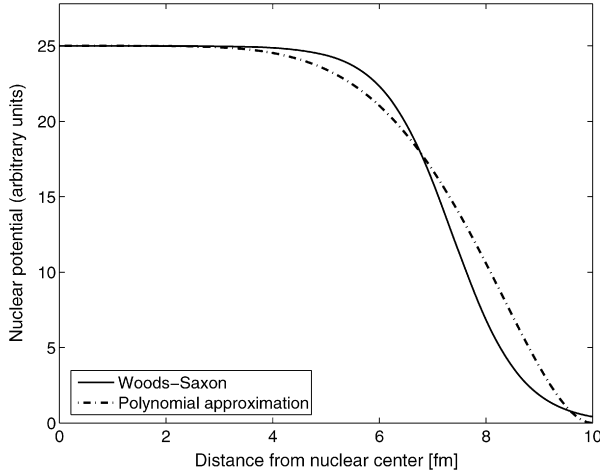


Fig. 1. Comparison of the Woods–Saxon type nuclear potential and the simple polynomial approximation described in the text, which allows to derive a simple analytic expression for the nuclear eikonal phase.

The approximate nuclear potential  $\tilde{V}_{\text{nuc}}(r, E)$  satisfies the boundary conditions  $\tilde{V}_{\text{nuc}}(R_{\text{max}}, E) = 0$  and  $\frac{d}{dr}\tilde{V}_{\text{nuc}}(R_{\text{max}}, E) = 0$ , which are acceptable for a distance of 10 fm from the nuclear center. A comparison of the exact Woods–Saxon distribution and approximation Eq. (26) is shown in Fig. 1. The contribution of  $\tilde{V}_{\text{nuc}}(r, E)$  to the eikonal phase of the nucleons can be derived from the integrals

$$\begin{aligned} \int (z^2 + b^2)^3 dz &= \frac{1}{7}z^7 + \frac{3}{5}b^2z^5 + b^4z^3 + b^6z, \\ \int \sqrt{z^2 + b^2} dz &= \left[ \frac{93}{128}b^6z + \frac{163}{192}b^4z^3 + \frac{25}{48}b^2z^5 + \frac{1}{8}z^7 \right] \\ &\quad \times \sqrt{z^2 + b^2} + \frac{35}{128}b^8 \log(z + \sqrt{z^2 + b^2}). \end{aligned} \quad (28)$$

In order to be compatible with [47], we used the electrostatic Coulomb potential generated by an homogeneously charged sphere ( $Z' = Z - 1$ ,  $R_C = 1.220A^{1/3} = 7.228$  fm)

$$V_{\text{coul}}(r) = \begin{cases} \frac{\alpha Z'}{R_C} \left( \frac{3}{2} - \frac{r^2}{2R_C^2} \right): & r \leq R_C, \\ \frac{\alpha Z'}{r}: & r \geq R_C, \end{cases} \quad (29)$$

for protons. The eikonal phase can easily be constructed from the expressions above, however one should note that the long-range part of the Coulomb potential must be regularized and one has ( $r'^2 = b^2 + z'^2$ ,  $r^2 = b^2 + z^2$ ,  $z = \hat{p}_i \vec{r}$ )

$$\begin{aligned} \chi_1^{\text{coul}}(\vec{r}) &= -\alpha Z' \frac{E_i}{|\vec{p}_i|} \lim_{R \rightarrow \infty} \left[ \int_{-\infty}^z \left( \frac{1}{r'} - \frac{1}{\sqrt{r'^2 + R^2}} \right) dz' - \log(R/R_0) \right] \\ &= -\alpha Z' \frac{E_i}{|\vec{p}_i|} \log\left( \frac{R_0(r+z)}{b^2} \right) \end{aligned} \quad (30)$$

or

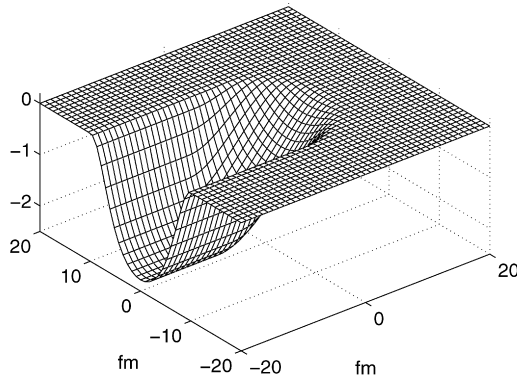


Fig. 2. Typical eikonal phase for outgoing neutrons in a plane through the nuclear center ( $\vec{p}_f$  points rearwards to the right). The plot shows  $\int_0^\infty V_{\text{nuc}}(\vec{r} + \hat{p}_f s) ds$ , where  $V_{\text{nuc}}(\vec{r})$  is an attractive Woods–Saxon potential with a depth given via  $V_{\text{WS}}(E) = 30$  MeV and corresponding parameters for  $^{208}\text{Pb}$ .

$$\begin{aligned} \chi_1^{\text{coul}}(\vec{r}) &= -\alpha Z' \frac{E_i}{|\vec{p}_i|} \log\left(\frac{R_0(r+z)}{r^2-z^2}\right) \\ &= \alpha Z' \frac{E_i}{|\vec{p}_i|} \log(k_i r - \vec{k}_i \vec{r}) + \text{const}, \end{aligned} \tag{31}$$

which is defined up to a constant phase given by the free parameter  $R_0$ . Analogously,  $\chi_2^{\text{coul}}$  which is relevant for our case is given in a space region where, e.g.,  $r > R_C$  and  $\hat{p}_f \vec{r} > 0$ , by

$$\begin{aligned} \chi_2^{\text{coul}}(\vec{r}) &= -\alpha Z' \frac{E_f}{|\vec{p}_f|} \log\left(\frac{R'_0(r-\tilde{z})}{\tilde{b}^2}\right) \\ &= \alpha Z' \frac{E_f}{|\vec{p}_f|} \log(k_f r + \vec{k}_f \vec{r}) \end{aligned} \tag{32}$$

with  $\tilde{z} = \hat{p}_f \vec{r}$  and  $\tilde{b}^2 = r^2 - \tilde{z}^2$ .

Figs. 2 and 3 show typical eikonal phases for neutrons (protons) in (a repulsive Coulomb and) a mean field optical potential for  $^{208}\text{Pb}$  with a depth of, e.g., 30 MeV. Note that the maximal depth of the surface in Fig. 2 is given approximately by the spatial extension of the Woods–Saxon potential multiplied by the potential depth, i.e.  $\sim 30 \text{ MeV} \times 14 \text{ fm} \simeq 2.13 \hbar c$ . The eikonal phases depicted in Figs. 2 and 3 must be multiplied, up to a sign, by a energy-dependent factor  $E_f/|\vec{p}_f| > 1$  in order to get the relevant phase which distorts the corresponding nucleon Dirac spinor.

In addition to the eikonal phase correction, we also took the (de-)focusing effect of the nucleon wave functions in the energy-dependent optical potential into account. We remark that Baker investigated the second-order eikonal approximation for potential scattering in the non-relativistic case [50], finding thereby an expression for the focusing factor of continuum Schrödinger wave functions. For a spherically symmetric potential  $V(r)$ , one finds for the central focusing factor  $f(0)$  of the amplitude of a non-relativistic scalar nucleon wave function (see Eq. (23) in [50])

$$f(0) \simeq 1 - \frac{V(0)}{2p_f v_f}, \tag{33}$$

where  $p_f$  is the asymptotic momentum and  $v_f$  the velocity of the particle. Roughly speaking, the approximation is valid if the asymptotic kinetic energy of the particle is larger than the depth

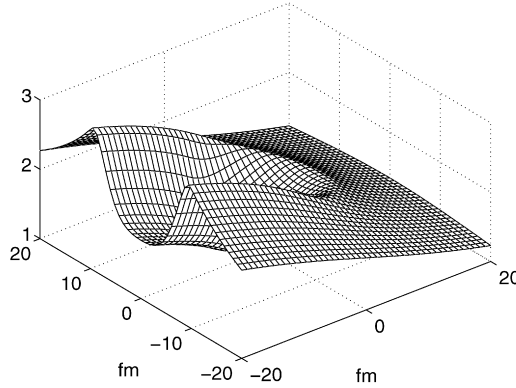


Fig. 3. Typical eikonal phase for outgoing protons in a plane through the nuclear center. The plot shows the regularized combined phase  $\mathcal{R} \int_0^\infty U(\vec{r} + \hat{p}_f s) ds$  with  $U(r) = V_{\text{nuc}}(r, E) + V_{\text{coul}}(r)$  for the same nuclear Woods–Saxon potential as in Fig. 2 and the repulsive electrostatic potential for  $^{208}\text{Pb}$  with  $Z' = 81$ .

of the disturbing potential  $m \gg E_{\text{kin}}^f = E_f - m \gg |V(0)|$ , and the wave length of the particle  $\sim 2\pi/p_f$  should be significantly smaller than the extension of the potential. For the classical particle momentum in the center of the potential  $p_f(0)$  one has non-relativistically

$$\begin{aligned} p_f(0) &= \sqrt{2m(E_{\text{kin}}^f - V(0))} \\ &= \sqrt{2mE_{\text{kin}}^f(1 - V(0)/E_{\text{kin}}^f)} \simeq p_f(1 - V(0)/2E_{\text{kin}}^f), \end{aligned} \quad (34)$$

such that

$$f(0) \simeq 1 - \frac{V(0)}{2p_f v_f} \simeq \sqrt{\frac{p_f(0)}{p_f}}, \quad (35)$$

i.e. it is found that the probability density is enhanced by the square root of the ratio of the central and asymptotic momenta  $p_f(0)/p_f$ , contrary to the result  $f(0) = p_f(0)/p_f \simeq (E_f - V(0))/E_f$  in the highly relativistic case. One may ask how the non-relativistic and the highly relativistic regime are connected. A classical relativistic analysis of the particle trajectories shows that the central focusing is given by the expression

$$f(0) = \left( \frac{p_f(0)}{p_f} \frac{E_f - V(0)}{E_f} \right)^{1/2}, \quad (36)$$

which interpolates between the non-relativistic and relativistic regime [51]. We additionally solved the Dirac equation for Dirac nucleons in the energy-dependent volume-central part of the optical potential used in this work for different energies, such that the amplitude of the eikonal phase corrected nucleon spinors could also be corrected by the corresponding energy-dependent amplitude modification.

The focusing and eikonal phase correction has an impact on the outgoing nucleon flux, and both the cross sections calculated in our approach and the results found in [30] agree in a different, but acceptable manner with the experimental data. An overall phenomenological Perey factor [52] (correcting for the violation of unitarity in our simplified approach) which applies in the same manner to the nucleon wave functions irrespective of the electron wave functions used, only leads to small corrections to the cross sections of the order of a few percent and has

been neglected. However, even though the distorted nucleon wave function approach presented in [30] is more ambitious than the present one, it is unable to reproduce the experimental data on a much higher level of precision, since it is still based on a SPS model, which fails to account for many physical aspects of the inclusive scattering process. A relevant observation presented in this paper is the fact that Coulomb corrections turn out to be compatible with the EMA, with no strong dependence on the nuclear models we used for the final state nucleons.

However, a critical remark should be made concerning the FSI. As mentioned above, an effect of the FSI is a reduction of the peak intensity and a certain broadening of the quasi-elastic peak. It is hoped that these modifications of the quasi-elastic scattering process affect the electron PWBA, EMA, and DWBA calculations in a similar way, such that an analogous comparison of the impact of the electron Coulomb distortion on  $(e, e')$  cross sections is still possible after FSI have been taken into account. The present calculations rely on a simplified picture of the nuclear current, which also neglects possible effects concerning the bound and final state nucleons as they are taken into account by, e.g., relativistic mean-field models for nuclear matter. The FSI are therefore not entirely under control and will modify our results to some extent. It is therefore highly desirable that this issue will be investigated in further detail in the near future.

It is clear that the same wave functions for the outgoing nucleon have to be used for the electron PWBA and exact DWBA calculations, since we are only interested in the role of the electronic part of the Coulomb corrections. As mentioned above, for bound nucleons wave functions generated from a non-relativistic Woods–Saxon potential and a Coulomb potential for the protons were used. The Woods–Saxon potential, which included an LS coupling term, was optimized in such a way that the experimental binding energies of the upper proton shells and the rms of the nuclear charge distribution were reproduced correctly. The rms radius of the neutron density distribution was taken from a recent study presented in [53], the binding energies, which also enter in the calculation of the wave functions of the outgoing protons and in the phase space factors, were taken from [54].

### 3.3. Electromagnetic nucleon current

The nucleon current

$$j_N^\mu = e \bar{\Psi}_{N,f} \hat{J}_N^\mu \Psi_{N,i}, \quad (37)$$

was modeled by using the *cc1* current introduced by de Forest, given by the operator [55]

$$\hat{J}_N^\mu(cc1) = (F_1 + \kappa F_2) \gamma^\mu - \frac{(p_i^\mu + p_f^\mu)}{2m_N} \kappa F_2, \quad (38)$$

with the so-called Dirac and Pauli form factors  $F_{1,2}(q^2)$  related to the Sachs form factors  $G_E(q^2)$ , and  $G_M(q^2)$  [56–58], according to

$$G_E(q^2) \equiv F_1(q^2) + \frac{\kappa q^2}{(2m)^2} F_2(q^2) = F_1(q^2) - \kappa \tau F_2(q^2), \quad (39)$$

$$G_M(q^2) \equiv F_1(q^2) + \kappa F_2(q^2), \quad (40)$$

where  $q^2 = (p_f^\mu - p_i^\mu)^2$ , and  $\kappa$  is the anomalous magnetic moment in units of nuclear magnetons ( $\kappa_p = \mu_p - 1 = 1.792847$  for the proton, and  $\kappa_n = \mu_n = -1.913043$  for the neutron). We emphasize that  $p_i^\mu$ ,  $p_f^\mu$  and correspondingly  $q^2$  are differential operators acting on the initial and final state nucleon wave functions  $\Psi_{N,f}$  and  $\Psi_{N,i}$ , and should not be confused naively

with corresponding asymptotic C-number momenta of the nucleon. However, for the sake of convenience, we maintain here this notational ambiguity, which is irrelevant in the case of free particles described by plane waves. We note that we used a completely analogous expansion of the  $q^2$ -dependence of the form factor operators as it was used by Knoll for the photon propagator in Eqns. (8)–(10) in our numerical calculations.

We adopted the dipole formula for the nucleon form factors according to

$$G_E^p(Q^2 = -q^2) = G_D(Q^2) = \left(1 + \frac{Q^2}{0.71 \text{ GeV}^2}\right)^{-2}, \quad (41)$$

with a magnetic proton form factor given by  $G_M^p(Q^2) = (1 + \kappa_p)G_E^p(Q^2)$ , or equivalently

$$F_1^p = \frac{1 + \mu_p \tau}{1 + \tau} G_E^p, \quad F_2^p = \frac{1}{1 + \tau} G_E^p. \quad (42)$$

In the case of the neutron we used the Galster parametrization [59] for the (small) electric form factor

$$G_E^n(Q^2) = -\tau \kappa_n G_D(Q^2) \xi_n(Q^2), \quad (43)$$

$$\xi_n(Q^2) = \left(1 + \frac{Q^2}{0.63 \text{ GeV}^2}\right)^{-1}, \quad (44)$$

consistent with the world data [60,61], and  $G_M^n(Q^2) = \kappa_n G_D(Q^2)$ , such that

$$F_1^n = \frac{G_E^n + \tau G_M^n}{1 + \tau}, \quad F_2^n = \frac{G_M^n - G_E^n}{\kappa_n(1 + \tau)}. \quad (45)$$

An alternative to the  $cc1$  current is the  $cc2$  current

$$\hat{J}_N^\mu(cc2) = F_1 \gamma^\mu + \frac{i\kappa}{2m_N} \sigma^{\mu\nu} q_\nu F_2, \quad (46)$$

which was also used in order to check how the ratio of the cross sections behaves for different models of the nuclear current. None of the expressions for the current ( $cc1$ ,  $cc2$ ) is fully satisfactory and both expressions fail to fulfill current conservation, but given the fact that we focus mainly on the electronic part of the problem, the simple choices given above provide a satisfactory description of the proton current. An advantage of the  $cc2$  choice is the fact that integration by parts allows one in a simple way to get rid of the momentum operators acting on the nucleon wave functions.

The asymptotic momenta of the nucleons were calculated from energy and momentum conservation, i.e. the energy of the knocked-out nucleons was reduced by their initial binding energies. We also performed calculations with enhanced binding energies in order to take into account that the average nucleon removal energy is higher than the average binding energy. This strategy leads to a shift of the quasi-elastic peak to higher energy transfer, but has no significant impact on the general conclusions drawn in this paper concerning the applicability of the EMA. We found in general that different choices for the nucleon current within the framework presented in this paper do not affect significantly the relative behavior of PWBA, EMA and DWBA calculations. This is not the case for the absolute cross section themselves.

The accuracy concerning the calculation of cross sections is limited to about 1% due to the truncation of the Knoll expansion Eq. (10) and the finite resolution of the grid that has been used for the modeling of the nucleus. The numerical evaluation of transition amplitudes was performed by putting the nucleus on a three-dimensional cubic grid with a side length of 30 fm and a grid

spacing of  $(30/n_{\text{grid}})$  fm, and convergence was checked by using different side lengths and grid resolutions. The number of necessary grid points  $\sim n_{\text{grid}}^3$  is mainly dictated by the wave length of the oscillatory behavior of the matrix element Eq. (9)  $\sim e^{i(\vec{k}_i - \vec{k}_f - \vec{p}_f)}$  and was in the range of  $70^3$  to  $130^3$  in order to ensure an accuracy better than  $10^{-1}$  percent for the values of the integrals. The accuracy of the solid angle integration of the  $(e, e'N)$  cross section was better than 0.05%. The truncation of the partial wave expansion of the electron wave functions [37] was performed such that all partial waves corresponding to angular momenta up to  $|\kappa| = 70$  were taken into account, which guaranteed an accurate evaluation of the electron wave functions and corresponding first and second order derivatives appearing in the Knoll expansion in the relevant nuclear vicinity.

#### 4. Results

We first discuss some phenomenological properties of the quasi-elastic peak, calculated within the electron PWBA, EMA, and DWBA SPS framework, and from an experimental point of view. Within a simplified picture like the Fermi gas model, the position of the quasi-elastic peak for  $(e, e')$  scattering with initial electron energy  $\epsilon_i$  and scattering angle  $\Theta_e$  is expected at

$$\omega_{\text{peak}} = \frac{Q_{\text{peak}}^2}{2m_N} + \bar{\epsilon}_{\text{rem}} = \frac{\epsilon_i^2(1 - \cos \Theta_e)}{m_N + (1 - \cos \Theta_e)\epsilon_i} + \bar{\epsilon}_{\text{rem}}, \quad (47)$$

where  $\bar{\epsilon}_{\text{rem}}$  can be interpreted as a phenomenological average removal energy of approximately 44 MeV [19]. These 44 MeV include a Coulomb shift of approximately 8 MeV, such that the physically relevant Coulomb corrected removal energy is rather given by  $\sim 36$  MeV, if the comparably small contribution of neutrons to the  $(e, e')$  cross section is not taken into account. The naive expression Eq. (47) predicts a difference of the position of the PWBA and EMA quasi-elastic peaks of 7.1 MeV for  $\epsilon_i = 485$  MeV and  $\Theta_e = 60^\circ$ , and 11.7 MeV for  $\epsilon_i = 310$  MeV and  $\Theta_e = 143^\circ$ . A fit of the experimentally measured peak positions [17,36] leads to

$$\omega_{\text{peak}}^{\text{exp}} = \frac{\epsilon_i'^2(1 - \cos \vartheta) + \tilde{m}_N \bar{E}}{\tilde{m}_N + \epsilon_i'(1 - \cos \vartheta)} \quad (48)$$

with  $\tilde{m}_N$  and  $\bar{E}$  as fitting parameters, and  $\epsilon_i' = \epsilon_i - \bar{V}$  is the effective initial electron energy with  $\bar{V} = -20$  MeV in the present fit. Eq. (48) incorporates also the background in the experimental data due to physical mechanisms like correlation effects and meson exchange currents which are not included in the SPS model. The experimental data are reproduced in a very satisfactory manner by Eq. (48) for  $\Theta_e = 60^\circ$  with  $\tilde{m}_N = 721$  MeV and  $\bar{E} = 12.8$  MeV in the energy range  $\epsilon_i = 262 \dots 645$  MeV, and for  $\Theta_e = 143^\circ$  with  $\tilde{m}_N = 662$  MeV and  $\bar{E} = 10.0$  MeV in the energy range  $\epsilon_i = 140 \dots 420$  MeV. From Eq. (48), one obtains a difference of the position of the PWBA and EMA quasi-elastic peaks of 8.3 MeV for  $\epsilon_i = 485$  MeV and  $\Theta_e = 60^\circ$ , and 13.4 MeV for  $\epsilon_i = 310$  MeV and  $\Theta_e = 143^\circ$ .

The corresponding calculations displayed in Figs. 4 and 5 (Figs. 6 and 7) based on the nuclear eikonal model (plane wave approximation) confirm the behavior of the quasi-elastic peak position described above in a satisfactory way. E.g., the peak shifts are 10.9 MeV (12.8 MeV) for the (310 MeV,  $143^\circ$ ) kinematics and 9.2 MeV (7.8 MeV) for the (485 MeV,  $60^\circ$ ) kinematics.

A further comment concerns the relative amplitude of the PWBA and EMA quasi-elastic peak. An analysis of the Saclay data shows that the maximal  $(e, e')$  peak cross section  $\sigma_{\text{peak}} = \frac{d^2\sigma}{d\omega d\Omega}|_{\omega_{\text{peak}}}$  scales like  $\sigma_{\text{peak}} \sim \epsilon_i^{-2.9}$  in the initial electron energy region  $\epsilon_i \sim 485$  MeV for

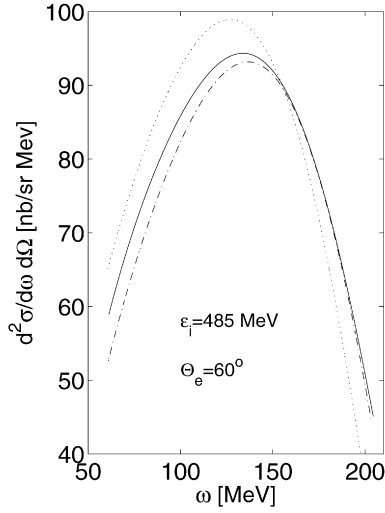


Fig. 4. The differential cross section for  $^{208}\text{Pb}(e, e')$  scattering for  $\epsilon_i = 485$  MeV and  $\Theta_e = 60^\circ$ , based on the eikonal approximation for the nuclear current. The dotted line is the electron PWBA result, the dash-dotted line shows the EMA result with an effective potential value  $\bar{V} = -19$  MeV, and the solid line displays the DWBA calculation.

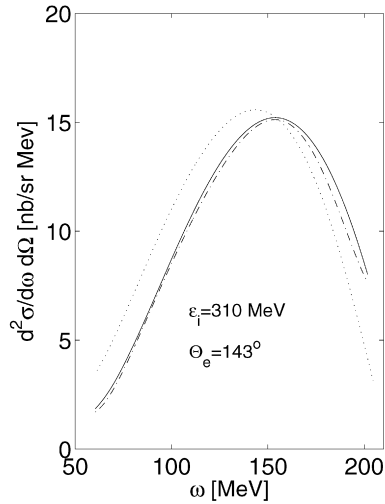


Fig. 5. The results corresponding to Fig. 4 for the (310 MeV,  $\Theta_e = 143^\circ$ ) kinematics.

$\Theta_e = 60^\circ$ . Since the EMA cross section can be obtained by multiplying the PWBA cross section, obtained from effective kinematic quantities, with a focusing factor  $[(\epsilon_i - \bar{V})/\epsilon_i]^2$ , a ratio of  $\sigma_{\text{peak}}^{\text{PWBA}}/\sigma_{\text{peak}}^{\text{EMA}} \simeq (504/485)^{0.9} = 1.035$  is expected for the PWBA and EMA peak values, if the theoretical model is in acceptable accordance with the properties of the physical nucleus. For  $\Theta_e = 143^\circ$ , the scaling behavior is  $\sim \epsilon_i^{-2.45}$  in the energy region  $\epsilon_i \sim 310$  MeV, predicting an approximate ratio  $\sigma_{\text{peak}}^{\text{PWBA}}/\sigma_{\text{peak}}^{\text{EMA}} \simeq (329/310)^{0.45} = 1.027$ , and  $\sim \epsilon_i^{-1.9}$  in the energy region  $\epsilon_i \sim 224$  MeV, such that the peak values of the PWBA and EMA cross section are nearly iden-



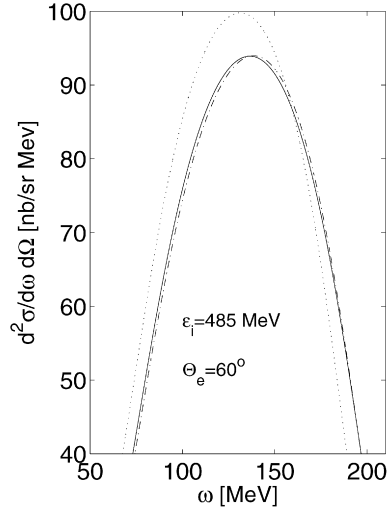


Fig. 6. The differential cross section for  $^{208}\text{Pb}(e, e')$  scattering at two different electron energies and scattering angles (see also Fig. 6), calculated by using plane wave functions for the final state nucleons (dotted line: PWBA, dash-dotted line: EMA with effective potential  $\tilde{V} = -19$  MeV, solid line: DWBA). The peaks are slightly narrower than in the nuclear eikonal model, since effects of the final state interactions described by the optical potential are absent.

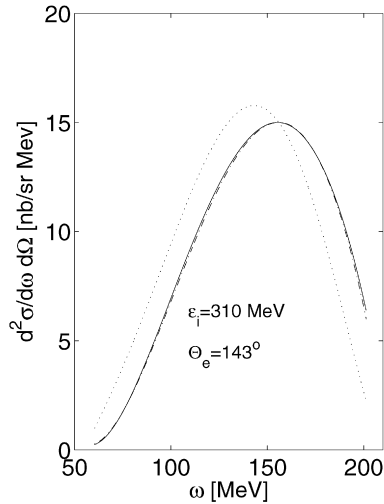


Fig. 7. The results corresponding to Fig. 6 for the (310 MeV,  $\theta_e = 143^\circ$ ) kinematics.

tical, as observed in Fig. 8. We note that the problematic ‘staircase-like’ behavior of the Saclay data, discussed in [21], has only a minor influence on the valuations presented above.

The relative amplitudes and the peak shifts presented in [30] do not exhibit the behavior expected from the discussion above in a distinct manner, even if one takes into account that a central potential value  $V(0) \simeq -25$  MeV has been used in [30] for the EMA, whereas an average potential value  $\tilde{V} = -19$  MeV has been used for our calculations presented in Figs. 4–8. Especially, a pronounced enhancement of the DWBA cross sections with respect to the EMA

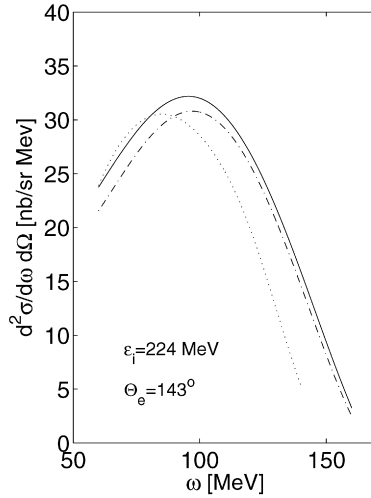


Fig. 8. PWBA, EMA and DWBA cross section for the (224 MeV,  $143^\circ$ ) kinematics (nucleon eikonal model,  $\bar{V} = -19$  MeV). The EMA fails to describe the DWBA cross sections reliably due to the low final state electron energy and the influence of the optical potential on the final state nucleons for low energy transfer.

cross sections in [30] is absent in the present calculations, except for the case where the final state electron energy is specifically low, as shown in Fig. 8.

For the (485 MeV,  $60^\circ$ ) kinematics, a slight shift to the left of the DWBA curve with respect to the EMA curve is observed. Still, an EMA-type behavior of the DWBA result can be noticed. For lower energy transfer, the influence of the optical potential on the nucleons with relatively low energy is stronger and becomes less important at higher energy transfer, where the EMA and DWBA match almost perfectly. The EMA/DWBA mismatch is virtually absent in the case where plane waves are used for the outgoing nucleon wave functions (see Figs. 6 and 7), i.e. when the distortion of the final state nucleons is not taken into account. From a practical point of view, one may observe that the EMA and the DWBA curve match almost perfectly in the energy range  $80 \text{ MeV} < \epsilon_i < 180 \text{ MeV}$ , if an effective potential value of  $-16$  MeV is used and the EMA results are additionally amplified by 2%. However, from the physical point of view, one should argue that an effective potential value of  $\bar{V} = -19$  MeV is an optimal choice, if the energy transfer and the corresponding energy of the final state nucleons is high enough such that the impact of the final state interaction on the cross described by the optical potential becomes less important. The DWBA cross sections are still larger by 1–2% than the EMA cross sections in this kinematical region, i.e., a slight ‘overfocusing’ can be observed. Still, one should keep in mind that the accuracy of the present calculations is limited to a similar order of magnitude by the use of the expansion Eq. (10). For the (310 MeV,  $143^\circ$ ) kinematics, the situation is similar, although the impact of the final state interaction described by the optical potential in the low energy transfer region to the left of the quasi-elastic peak is less pronounced. This is also due to the fact that a marginally larger effective potential of 20 MeV would be appropriate for this kinematics, leading to a better fit of the EMA and DWBA for higher energy transfer. Furthermore, the quasi-elastic peak is also shifted to higher energy transfer compared to the (485 MeV,  $60^\circ$ ) kinematics, additionally reducing the influence of the optical potential.

As expected, in the case of the (224 MeV,  $143^\circ$ ) kinematics displayed in Fig. 8, the EMA starts to fail. The reason is twofold. Firstly, the energy of the final state electrons is relatively small, and

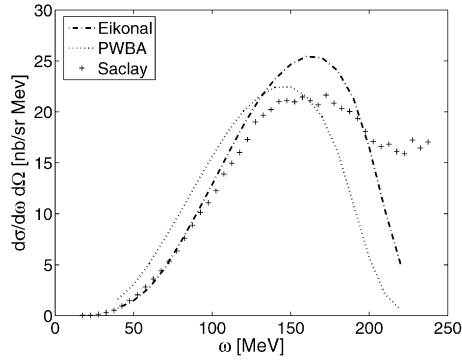


Fig. 9. Cross sections for  $(e, e')$  scattering with  $\epsilon_i = 310$  MeV and  $\vartheta = 143^\circ$  obtained in [34]. The plots displays a similar behavior as the results presented in [30], however, the Coulomb corrected eikonal cross sections are too large due an overestimation of the electron wave function focusing. A slightly different nuclear model was used than in the present work, and the reduced strength due to correlated nucleons had been neglected.

the focusing effect becomes more important [51], such that the DWBA cross section becomes significantly larger than the EMA prediction. Secondly, the quasi-elastic peak is shifted towards smaller energy transfer, where the optical potential increasingly distorts the wave functions of the final state nucleons. The momentum transfer squared is still relatively large, and is therefore not a contributing factor to the failure of the EMA. Note also that the shifts of the EMA and DWBA peaks with respect to the PWBA peak are still of comparable size. Again, in order to describe the DWBA result within an EMA framework, one could increase the effective potential to a higher value such that the EMA and DWBA curve match better in the region of large energy transfer. An other strategy would be to derive an optimized effective potential which shifts the maximum of the EMA and DWBA peak to the same position and to renormalize the EMA curve by an appropriate factor subsequently.

As a general remark, one may observe that the Coulomb corrections introduced within the framework of the asymptotic expansion Eq. (10) according to Knoll depend on derivatives of the electron charge and current densities, or, by partial integration, on the nuclear four-current. Since the corresponding nuclear response is rather smooth (differently from elastic and transition form factors to discrete levels), and only leading terms in the expansion are relevant, one could expect that the dependence of Coulomb effects on different models of the nuclear current is rather weak.

We finally comment on the electron eikonal calculations (EDWBA) presented in [34], which originally seemed to be compatible with the Ohio group results in [30]. The PWBA and EDWBA curves in Fig. 3 of [34] show a indeed similar behavior as the PWBA and DWBA results in [30]. As in [30], the Coulomb corrected cross section is larger at the peak than in the PWBA case, seemingly in contradiction with the EMA. A typical example from [34] is displayed in Fig. 9, where also experimental data taken at Saclay have been included [17]. However, there is a simple explanation for this discrepancy. For the EDWBA calculations in [34], a focusing value for the electron cross section was used which corresponds basically to the central value of the electrostatic potential, i.e.  $V(0) = 25$  MeV, which leads to an overestimation of the Coulomb corrected cross sections. Note that the average momentum of the electrons is well described by the eikonal integral and also corresponds also to an average value of approximately 19 MeV.

Therefore, the results presented in [34] can be corrected by implementing the focusing of the electron wave functions obtained from the exact electron wave functions in the program

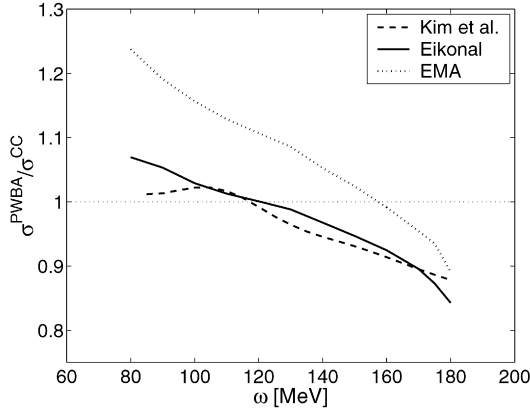


Fig. 10. Comparison of Coulomb corrections ( $\epsilon_i = 485$  MeV,  $\vartheta = 60^\circ$ ) for different approaches in [34]. For the EMA, an effective potential value of 25 MeV was used.

originally used in [34], with the result illustrated below for Fig. 4 in [34], which is displayed again as Fig. 10 in this paper. The figure shows the ratio of the cross sections, calculated in PWBA, with the Coulomb corrected cross sections according to the EDWBA and EMA. Firstly, the EMA curve has to be adapted to an effective potential of 19 MeV instead of 25 MeV. This slightly reduces the ratio  $\sigma_{\text{PWBA}}/\sigma_{\text{EMA}}$  and moves the corresponding dotted curve closer to one (the horizontal line). Secondly, the focusing factors of the EDWBA calculations must be corrected. E.g., for  $\epsilon_i = 485$  MeV and  $\epsilon_f = 385$  MeV, the total focusing factor entering the EDWBA for the initial and final state electron originally used in [34] corresponded approximately to the numerical value

$$\frac{(485 + 25)^2 \times (385 + 25)^2}{485^2 \times 385^2} \simeq 1.254. \quad (49)$$

The correct total focusing factor should rather be

$$\frac{(485 + 19)^2 \times (385 + 19)^2}{485^2 \times 385^2} \simeq 1.189. \quad (50)$$

Accordingly, the EDWBA cross section has to be reduced by 5.2% at  $\omega = 100$  MeV and the corresponding solid curve moves upwards in the plot. The consequences are shown in Fig. 11. Note that for Fig. 11, also locally varying focusing factors obtained from exact solutions of the Dirac equation were used in conjunction with the eikonal approximation for the phase of the electron wave functions. An attempt to calculate corrections to the focusing at some distance to the nuclear center has already been presented in [62], which, however, does not lead to reliable predictions in the important surface region of the nucleus and resulted in the overestimation of the focusing in [34]. For the EMA calculation presented in Fig. 11, a slightly smaller value  $\bar{V} = 18.7$  MeV than in the calculational example above was used, since this value has been determined experimentally to be  $\bar{V} = 18.7 \pm 1.5$  MeV for  $^{208}\text{Pb}$  [18] by a comparison of inclusive electron and positron scattering data. This independent experimental finding is remarkable, since it also supports that an effective potential which is slightly smaller than the naive mean potential  $\bar{V} \sim 4V(0)/5 \sim 20$  MeV is adequate. One might speculate that the contribution of nucleons near the surface of the nucleus to inclusive scattering is enhanced, leading to the observed reduction of the effective potential.

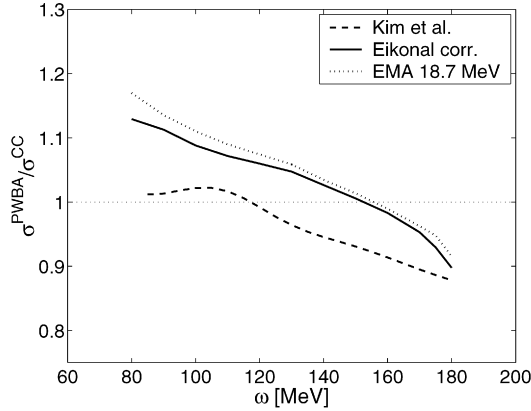


Fig. 11. The same as in Fig. 10, but with corrected focusing in the eikonal calculation and an EMA curve obtained by using an average potential  $\bar{V} = 18.7$  MeV.

## 5. Conclusions

As a basic result of this work we conclude that the EMA with an effective potential  $\hat{V} = -19$  MeV is a valid approximation for the description of Coulomb distortions in the kinematic region where the momentum transfer squared is larger than  $(300 \text{ MeV})^2$  (such that the length scale of the exchanged photon is smaller than the typical size of a nucleus), the energy of the scattered electron is larger than 150 MeV (such that the semiclassical description of the electron wave functions in the nuclear vicinity is valid) and the energy transfer  $\omega = \epsilon_i - \epsilon_f$  is larger than  $\sim 140$  MeV (such that the distortion of the final state nucleon wave functions is moderate). In the case mentioned above, and for a typical energy range where the initial electron energy is of the order of some hundreds of MeV, the DWBA cross sections are generally larger by 1–2% than the EMA cross sections. If the energy transfer  $\omega$  is smaller than 140 MeV, the DWBA cross section can still be approximated by an EMA calculation with a phenomenological effective potential  $\hat{V}$  and a minor amplitude correction. However, in such a case one has to rely on the model used to describe the nuclear current.

Other kinematic situations than those presented in this paper have been investigated, which showed that the behavior of the forward and backward scattering angle kinematics presented in this paper is typical.

The coincidence of EMA and DWBA cross sections is rather impressive. As a test, the PWBA and EMA cross section calculations which are based on plane Dirac waves for electrons were evaluated by both using Dirac plane waves and by performing a limit  $Z \rightarrow 0$  in the full Coulomb solver for the electron wave functions. Performing such a limit in the DWBA solver leads to the same cross sections as obtained from the plane wave calculations, such that the observed coincidence served as a numerical test for the two unrelated calculational techniques.

It is instructive to compare Fig. 4 in this work to Fig. 16 in the classic work by Rosenfelder on quasi-elastic electron scattering on nuclei [63]. It should be noted that Rosenfelder explicitly mentioned already in his work that the effective potential  $\bar{V}$  is close to the *mean value* of the electrostatic potential of the nucleus. However, he then wrote down the explicit expression for the *central value*

$$V(0) = -\frac{3Z\alpha}{2R} \quad (51)$$

of the potential of a homogeneously charged sphere with radius  $R$ , which is related to the corresponding mean value by  $\bar{V} \simeq 4V(0)/5$ . This minor, but not irrelevant misapprehension for the case of the EMA, has propagated in the literature since then (see, e.g., [6]). Apart from the fact that the initial electron energy is marginally larger and the effective potential used by Rosenfelder is given by  $\bar{V} = -24.9$  MeV, Fig. 16 in [63] can directly be related to the result presented in Fig. 4.

Despite many theoretical and experimental efforts to clarify to what extent a suppression of the Coulomb sum rule exists, clear answers to the problem are still missing. The origin of the discrepancy between the results presented in this paper and the findings of the Ohio group remains hitherto unclear, but one may speculate that it could be related to the relativistic nucleon potential model used by the Ohio group, which may influence the resulting nuclear current (spinor distortion or negative energy contributions) in an unexpected way. An overview on different theoretical attempts to implement Coulomb corrections in the analysis of experimental data can be found in [64]. According to a reanalysis of experimental data based on the validity of the EMA, which is supported by the present work, Meziani and Morgenstern claimed that a suppression of the longitudinal structure function of about 40% exists at the effective momentum transfer of 500 MeV/ $c$ , and tried to explain the suppression by a change of the nucleon properties inside the nuclear medium [22]. However, in view of the fact that theoretical questions about the interpretation of relativistic nucleon potential models persist and further related effects like meson exchange currents and correlations have not been taken into account in a satisfactory manner in theoretical Coulomb distortion calculations up to the present, and since the quality of experimental data may be questionable in some cases (see, e.g., [21]), it is advisable to await for the expected experimental TJNAF results at the high momentum transfer region, in which the relevant correlations become small, whereas Coulomb corrections become crucial to extract information about the structure functions and to understand the Coulomb sum rule.

## Appendix A

The nuclear charge distribution and nucleon optical potentials of heavy nuclei are often approximated by the help of a Woods–Saxon distribution. Normalizations and moments of Woods–Saxon distributions are rarely found in the literature, however, they can be expressed exactly in terms of polylogarithms.

The volume integral over the Woods–Saxon distribution with a range  $\tilde{r}$  and diffusivity  $a$

$$\rho(r) = \frac{\rho_0}{1 + e^{(r-\tilde{r})/a}} \quad (\text{A.1})$$

can be written with help of the trilogarithm

$$4\pi \int_0^\infty r^2 \rho(r) dr = -8\pi a^3 \rho_0 \text{Li}_3(-e^{\tilde{r}/a}) \rightarrow \frac{4}{3}\pi \tilde{r}^3 \rho_0 \quad (a \rightarrow 0), \quad (\text{A.2})$$

where the polylogarithms  $\text{Li}_n$  are defined for  $|z| < 1$  by

$$\text{Li}_n(z) = \sum_{k=1}^{\infty} \frac{z^k}{k^n}. \quad (\text{A.3})$$

For  $|z| > 1$ , the analytic continuation of the dilogarithm  $\text{Li}_2(z)$  and the trilogarithm  $\text{Li}_3(z)$  can be obtained via the functional equations

$$\text{Li}_2(z) = -\text{Li}_2(1/z) - \frac{1}{2} \log(-z)^2 - \frac{\pi^2}{6}, \quad (\text{A.4})$$

$$\text{Li}_3(z) = \text{Li}_3(1/z) - \frac{1}{6} \log(-z)^3 - \frac{1}{6} \pi^2 \log(-z). \quad (\text{A.5})$$

For a nucleus with charge number  $Z$  and total charge  $eZ$  one has

$$\rho_0 = -\frac{eZ}{8\pi a^3 \text{Li}_3(e^{-\tilde{r}/a})}. \quad (\text{A.6})$$

The potential energy of an electron in the center of the nucleus is given by

$$\begin{aligned} v_0 &= -e \int_0^\infty \rho(r) r dr = -ea^2 \rho_0 \text{Li}_2(-e^{\tilde{r}/a}) \\ &= \frac{\alpha Z \text{Li}_2(-e^{\tilde{r}/a})}{2a \text{Li}_3(-e^{\tilde{r}/a})}, \end{aligned} \quad (\text{A.7})$$

and the rms radius of the distribution is given by

$$\langle r^2 \rangle = 12a^2 \frac{\text{Li}_5(-e^{\tilde{r}/a})}{\text{Li}_3(-e^{\tilde{r}/a})}. \quad (\text{A.8})$$

This follows also from the general expression for the moments of the Woods–Saxon distribution

$$\frac{1}{n!} \int_0^\infty \frac{r^n}{1 + e^{(r-\tilde{r})/a}} dr = -a^{n+1} \text{Li}_{n+1}(-e^{\tilde{r}/a}). \quad (\text{A.9})$$

Note that the corresponding expressions for a homogeneously charged sphere can be obtained from the limit  $a \rightarrow 0$  and

$$\text{Li}_n(-e^x) \simeq -\frac{x^n}{n!} \quad \text{for } x > n^2. \quad (\text{A.10})$$

Choosing the typical parameters  $\tilde{r} = 6.6$  fm and diffusivity  $a = 0.545$  fm for the electric charge distribution of a  $^{208}\text{Pb}$  nucleus with mass number  $A = 208$  and charge number  $Z = 82$ , one finds that these values are compatible with an rms charge radius of 5.50 fm and a central Coulomb potential of  $V_0 = -25.71$  MeV.

## References

- [1] D.T. Baran, B.F. Filippone, D. Geesaman, M. Green, R.J. Holt, H.E. Jackson, J. Jourdan, R.D. McKeown, R.G. Milner, J. Morgenstern, D.H. Potterveld, R.E. Segel, P. Seidl, R.C. Walker, B. Zeidman, Phys. Rev. Lett. 61 (1988) 400–403.
- [2] J.P. Chen, Z.-E. Meziani, D. Beck, G. Boyd, L.M. Chinitz, D.B. Day, L.C. Dennis, G. Dodge, B.W. Filippone, K.L. Giovanetti, J. Jourdan, K.W. Kemper, T. Koh, W. Lorenzon, J.S. McCarthy, R.D. McKeown, R.G. Milner, R.C. Minehart, J. Morgenstern, J. Mougey, D.H. Potterveld, O.A. Rondon-Aramayo, R.M. Sealock, L.C. Smith, S.T. Thornton, R.C. Walker, C. Woodward, Phys. Rev. Lett. 66 (1991) 1283–1286.
- [3] Z.-E. Meziani, J.P. Chen, D. Beck, G. Boyd, L.M. Chinitz, D.B. Day, L.C. Dennis, G.E. Dodge, B.W. Fillipone, K.L. Giovanetti, J. Jourdan, K.W. Kemper, T. Koh, W. Lorenzon, J.S. McCarthy, R.D. McKeown, R.G. Milner, R.C. Minehart, J. Morgenstern, J. Mougey, D.H. Potterveld, O.A. Rondon-Aramayo, R.M. Sealock, I. Sick, L.C. Smith, S.T. Thornton, R.C. Walker, C. Woodward, Phys. Rev. Lett. 69 (1992) 41–44.
- [4] R. Altemus, A. Cafolla, D. Day, J.S. McCarthy, R.R. Whitney, J.E. Wise, Phys. Rev. Lett. 44 (1980) 965–968.

- [5] M. Deady, C.F. Williamson, J. Wong, P.D. Zimmerman, C. Blatchley, J.M. Finn, J. LeRose, P. Sioshansi, R. Altemus, J.S. McCarthy, R.R. Whitney, *Phys. Rev. C* 28 (1983) 631–634.
- [6] A. Hotta, P.J. Ryan, H. Ogino, B. Parker, G.A. Peterson, R.P. Singhal, *Phys. Rev. C* 30 (1984) 87–96.
- [7] M. Deady, C.F. Williamson, P.D. Zimmerman, R. Altemus, R.R. Whitney, *Phys. Rev. C* 33 (1986) 1897–1904.
- [8] C.C. Blatchley, J.J. LeRose, O.E. Pruet, P.D. Zimmerman, C.F. Williamson, M. Deady, *Phys. Rev. C* 34 (1986) 1243–1247.
- [9] S.A. Dytman, A.M. Bernstein, K.I. Blomqvist, T.J. Pavel, B.P. Quinn, R. Altemus, J.S. McCarthy, G.H. Mechtel, T.S. Ueng, R.R. Whitney, *Phys. Rev. C* 38 (1988) 800–812.
- [10] K. Dow, S. Dytman, D. Beck, A. Bernstein, I. Blomqvist, H. Caplan, D. Day, M. Deady, P. Demos, W. Dodge, G. Dodson, M. Farkhondeh, J. Flanz, K. Giovanetti, R. Goloskie, E. Hallin, E. Knill, S. Kowalski, J. Lightbody, R. Lindgren, X. Maruyama, J. McCarthy, B. Quinn, G. Retzlaff, W. Sapp, C. Sargent, D. Skopik, I. The, D. Tieger, W. Turchinets, T. Ueng, N. Videla, K. von Reden, R. Whitney, C. Williamson, *Phys. Rev. Lett.* 61 (1988) 1706–1709.
- [11] T.C. Yates, C.F. Williamson, W.M. Schmitt, M. Osborn, M. Deady, P.D. Zimmerman, C.C. Blatchley, K.K. Seth, M. Sarmiento, B. Parker, Y. Jin, L.E. Wright, D.S. Onley, *Phys. Lett. B* 312 (1993) 382–387.
- [12] C. Williamson, T.C. Yates, W.M. Schmitt, M. Osborn, M. Deady, P.D. Zimmerman, C.C. Blatchley, K.K. Seth, M. Sarmiento, B. Parker, Y. Jin, L.E. Wright, D.S. Onley, *Phys. Rev. C* 56 (1997) 3152–3172.
- [13] P. Barreau, M. Bernheim, J. Duclos, J.M. Finn, Z.-E. Meziani, J. Morgenstern, J. Mougey, D. Tarnowski, S. Turck-Chièze, M. Brussel, G.P. Capitani, E. De Sanctis, S. Frullani, F. Garibaldi, D.B. Isabelle, E. Jans, I. Sick, P.D. Zimmerman, *Nucl. Phys. A* 402 (1983) 515–540.
- [14] Z.-E. Meziani, P. Barreau, M. Bernheim, J. Morgenstern, S. Turck-Chièze, R. Altemus, J. McCarthy, L.J. Orphanos, R.R. Whitney, G.P. Capitani, E. De Sanctis, S. Frullani, F. Garibaldi, *Phys. Rev. Lett.* 52 (1984) 2130–2133.
- [15] Z.-E. Meziani, P. Barreau, M. Bernheim, J. Morgenstern, S. Turck-Chièze, R. Altemus, J. McCarthy, L.J. Orphanos, R.R. Whitney, G.P. Capitani, E. De Sanctis, S. Frullani, F. Garibaldi, *Phys. Rev. Lett.* 54 (1985) 1233–1236.
- [16] C. Marchand, P. Barreau, M. Bernheim, P. Bradu, G. Fournier, Z.-E. Meziani, J. Miller, J. Morgenstern, J. Picard, B. Saghai, S. Turck-Chièze, P. Vernin, *Phys. Lett. B* 153 (1985) 29–32.
- [17] A. Zghiche, J.F. Danel, M. Bernheim, M.K. Brussel, G.P. Capitani, E. De Sanctis, S. Frullani, F. Garibaldi, A. Gerard, J.M. Le Goff, A. Magnon, C. Marchand, Z.-E. Meziani, J. Morgenstern, J. Picard, D. Reffay-Pikeroen, M. Traini, S. Turck-Chièze, P. Vernin, *Nucl. Phys. A* 572 (1994) 513–559;
- A. Zghiche, J.F. Danel, M. Bernheim, M.K. Brussel, G.P. Capitani, E. De Sanctis, S. Frullani, F. Garibaldi, A. Gerard, J.M. Le Goff, A. Magnon, C. Marchand, Z.-E. Meziani, J. Morgenstern, J. Picard, D. Reffay-Pikeroen, M. Traini, S. Turck-Chièze, P. Vernin, *Nucl. Phys. A* 584 (1995) 757, Erratum.
- [18] P. Guèye, M. Bernheim, J.F. Danel, J.E. Ducret, L. Lakéhal-Ayat, J.M. Le Goff, A. Magnon, C. Marchand, J. Morgenstern, J. Marroncle, P. Vernin, A. Zghiche-Lakéhal-Ayat, V. Breton, S. Frullani, F. Garibaldi, F. Ghio, M. Iodice, D.B. Isabelle, Z.-E. Meziani, E. Offermann, M. Traini, *Phys. Rev. C* 60 (1999) 044308.
- [19] R.R. Whitney, I. Sick, J.R. Ficenec, R.D. Kephart, W.P. Trower, *Phys. Rev. C* 9 (1974) 2230–2235.
- [20] O. Benhar, A. Fabrocini, S. Fantoni, I. Sick, *Phys. Lett. B* 343 (1995) 47–52.
- [21] J. Jourdan, *Nucl. Phys. A* 603 (1996) 117–160.
- [22] J. Morgenstern, Z.-E. Meziani, *Phys. Lett. B* 515 (2001) 269–275.
- [23] D. Day, J.S. McCarthy, T.W. Donnelly, I. Sick, *Annu. Rev. Nucl. Part. Sci.* 40 (1990) 357–410.
- [24] D.B. Day, J.S. McCarthy, Z.-E. Meziani, R.C. Minehart, R.M. Sealock, S.T. Thornton, J. Jourdan, I. Sick, B.W. Filippone, R.D. McKeown, R.G. Milner, D.H. Potterveld, Z. Szalata, *Phys. Rev. C* 40 (1989) 1011–1024.
- [25] H. Überall, *Electron Scattering from Complex Nuclei*, Academic Press, New York, 1971.
- [26] G. Co', J. Heisenberg, *Phys. Lett. B* 197 (1987) 489–492.
- [27] M. Traini, S. Turck-Chièze, in: *Proceedings of the Fifth Mini-conference, Amsterdam, 19–20 November 1987*, p. 124.
- [28] M. Traini, S. Turck-Chièze, A. Zghiche, *Phys. Rev. C* 38 (1988) 2799;
- M. Traini, *Phys. Lett. B* 213 (1988) 1.
- [29] A. Aste, K. Hencken, D. Trautmann, *Eur. Phys. J. A* 21 (2004) 161–167.
- [30] K.S. Kim, L.E. Wright, Y. Jin, D.W. Kosik, *Phys. Rev. C* 54 (1996) 2515–2524.
- [31] J.M. Udias, J.R. Vignote, E. Moya de Guerra, A. Escuderos, J.A. Caballero, Recent developments in relativistic models for exclusive  $A(e, e' p)B$  reactions, in: *5th Workshop on “e – m Induced Two-Hadron Emission”*, Lund, 13–16 June 2001.
- [32] J.M. Udias, P. Sarriguren, E. Moya de Guerra, E. Garrido, J.A. Caballero, *Phys. Rev. C* 48 (1993) 2731–2739.
- [33] M. Traini, *Nucl. Phys. A* 694 (2001) 325–336.
- [34] A. Aste, K. Hencken, J. Jourdan, I. Sick, D. Trautmann, *Nucl. Phys. A* 743 (2004) 259–282.



- [35] A. Aste, J. Jourdan, *Europhys. Lett.* 67 (2004) 753–759.
- [36] A. Aste, *nucl-th/0611100*.
- [37] A. Aste, C. von Arx, D. Trautmann, *Eur. Phys. J. A* 26 (2005) 167–178.
- [38] Y. Horikawa, F. Lenz, N.C. Mukhopadhyay, *Phys. Rev. C* 22 (1980) 1680–1695.
- [39] O. Benhar, A. Fabrocini, S. Fantoni, G.A. Miller, V.R. Pandharipande, I. Sick, *Phys. Rev. C* 44 (1991) 2328–2342.
- [40] M. Goepfert-Mayer, *Phys. Rev.* 75 (1949) 1969–1970.
- [41] J. Knoll, *Nucl. Phys. A* 201 (1973) 289–300.
- [42] C. Giusti, F.D. Pacati, *Nucl. Phys. A* 473 (1987) 717–735.
- [43] A. Aste, D. Trautmann, *Eur. Phys. J. A* 33 (2007) 11–20.
- [44] O. Benhar, A. Fabrocini, S. Fantoni, *Nucl. Phys. A* 505 (1989) 267–299.
- [45] I. Sick, *Prog. Part. Nucl. Phys.* 59 (2007) 447–454.
- [46] J.M. Udias, J.A. Caballero, E. Moya de Guerra, J.E. Amaro, T.W. Donnelly, *Phys. Rev. Lett.* 83 (1999) 5451–5454.
- [47] A.J. Koning, J.P. Delaroche, *Nucl. Phys. A* 713 (2003) 231–310.
- [48] V. Lukyanov, E. Zemlyanaya, *J. Phys. G: Nucl. Part. Phys.* 26 (2000) 357–363.
- [49] J.R. Shepard, E. Rost, *Phys. Rev. C* 25 (1982) 2660–2679.
- [50] A. Baker, *Phys. Rev. D* 6 (1972) 3462–3469.
- [51] A. Aste, D. Trautmann, *Eur. Phys. J. A* 33 (2007) 11–20.
- [52] S. Perey, B. Buck, *Nucl. Phys.* 32 (1962) 353–380.
- [53] B.C. Clark, L.J. Kerr, S. Hama, *Phys. Rev. C* 67 (2003) 054605.
- [54] M. van Batenburg, *Deeply-bound protons in  $^{208}\text{Pb}$* , Ph.D. thesis, University of Utrecht, Netherlands, 2001.
- [55] T. de Forest Jr., *Nucl. Phys. A* 392 (1983) 232–248.
- [56] G. Höhler, E. Pietarinen, I. Sabba-Stevescu, F. Borkowski, G.G. Simon, V.H. Walter, R.D. Wendling, *Nucl. Phys. B* 144 (1976) 505–534.
- [57] I. Qattan, J. Arrington, R.E. Segel, X. Zheng, K. Aniol, O.K. Baker, R. Beams, E.J. Brash, J. Calarco, A. Camsonne, J.P. Chen, M.E. Christy, D. Dutta, R. Ent, S. Frullani, D. Gaskell, O. Gayou, R. Gilman, C. Glashauser, K. Hafidi, J.-O. Hansen, D.W. Higinbotham, W. Hinton, R.J. Holt, G.M. Huber, H. Ibrahim, L. Jisonna, M.K. Jones, C.E. Keppel, E. Kinney, G.J. Kumbartzki, A. Lung, D.J. Margaziotis, K. McCormick, D. Meekins, R. Michaels, P. Monaghan, P. Moussiegt, L. Pentchev, C. Perdrisat, V. Punjabi, R. Ransome, J. Reinhold, B. Reitz, A. Saha, A. Sarty, E.C. Schulte, K. Slifer, P. Solvignon, V. Sulkosky, K. Wijesooriya, B. Zeidman, *Phys. Rev. Lett.* 94 (2005) 142301.
- [58] H. Castillo, C.A. Dominguez, M. Loewe, *JHEP* 0503 (2005) 012.
- [59] S. Galster, H. Klein, J. Moritz, K.H. Schmidt, D. Wegener, J. Bleckwenn, *Nucl. Phys. B* 32 (1971) 221–237.
- [60] S. Platchkov, A. Amroun, S. Auffret, J.M. Cavedon, P. Dreux, J. Duclos, B. Frois, D. Goutte, H. Hachemi, J. Martino, X.H. Phan, *Nucl. Phys. A* 510 (1990) 740–758.
- [61] T.W. Donnelly, M.J. Musolf, W.M. Alberico, M.B. Barbaro, A. De Pace, A. Molinari, *Nucl. Phys. A* 541 (1992) 525–577.
- [62] J. Knoll, *Nucl. Phys. A* 223 (1974) 462–476.
- [63] R. Rosenfelder, *Ann. Phys.* 128 (1980) 188–240.
- [64] K.S. Kim, B.G. Yu, M.K. Cheoun, *Phys. Rev. C* 74 (2006) 067601.